The Fracture Toughness of the Welding Zone in Gas Transfer Steel Pipes by Experimental and Numerical Methods

M.R. Torshizian [*], M. Boustani

Mechanical Engineering Department, Mashhad Branch, Islamic Azad University, Mashhad, Iran

ABSTRACT

Fracture toughness is a criterion to determine the resistance of materials against small longitudinal and peripheral cracks, which can be created in the effect of welding or peripheral effects. Therefore, it is extremely important to scrutiny the factors that impress crack treatment and the way that it grows. In this research, fracture toughness was investigated on the peripheral welding zone in gas and oil transfer pipelines made in steel API X65. The fracture toughness is derived by using two different methods. At first, the three-point bending test method was used on samples that made up of the peripheral welding zone. Then, with a numerical simulation it was calculated by ABAQUS software v6/10. The comparison of experimental results and computer simulation results shows good agreement from two methods. The fracture toughness of the welded zone, obtained in this study, was compared with that of the base metal. The results showed that fracture toughness on the welding zone in gas and oil transfer steel pipelines decreased 43% compared to the base metal. This issue shows that peripheral welding on gas and oil transfer pipelines has more talent for crack growth compared to the base metal.

© 2022 IAU, Arak Branch. All rights reserved.

Keywords: Fracture toughness; Gas and oil pipeline; Three-point bending test; Abaqus software.

1 INTRODUCTION

STEEL pipes are one of the most important methods for gas transfer in the world. In recent years, the use of a high-pressure pipeline of gas and oil, with more capacity, has developed. This kind of structure is designed to tolerate internal pressure between 10-15 *MPa* equal to 75-80% of the minimum of steel nominal stress. According to the necessity of safe design for natural gas transfer via steel pipelines in working conditions, it is essential to have full information from this type of steel. Cracks may occur during pipe welding operations; it is one of the factors that can cause problems in these pipes. Also, it is important and essential that the effect of crack must be investigated on the strength of the welding zone and growth of the crack. Shin and Park [1] simulated tension crack growth on steam

_____

[*]Corresponding author. Tel.: +98 915 5000609.
E-mail address: torshizian@mshdiau.ac.ir (M.R. Torshizian)

JOURNAL OF SOLID MECHANICS JSM

transmission pipes by ANSYS software. Kamaya and Takayuki [2] examined the impress of several tiny cracks on crack growth and showed that environmental conditions are one of the effective factors on results. They used crack simulation and experimental tests to get more information with modified crack simulation and decreased calculation. Lee et al. [3] investigated crack safety on base and welding metal. Their samples, which were gas transfer steel pipelines, had a longitudinal crack on the external crust. Oh et al. [4] presented a model of ductile fracture for the API X65 steel. Experimental tests and finite element simulations were performed to predict the pre-strain effect on deformation and fracture. Beak et al. [5] studied the influence of pre-strain on mechanical properties of the API 5L X65 pipe with large plastic deformation. The results showed that tensile and yield strength increased with increasing tensile pre-strain. Ben Amar et al. [6] investigated the resistance to ductile crack extension. They used a numerical method for simulations of crack propagation and arrest. Results were presented on a pipe made in steel API L X65. Sirin et al. [7] discussed the effect of different chemical compositions of API X65 steel and weld electrodes on the mechanical properties of steel welds. Maksuti et al. [8] studied the microstructure properties of the welded joint in pipeline steel API X65. The welded joint was produced by two-pass submerged arc welding. The toughness behavior of the base metal, weld metal, and heat-affected zone were investigated. Mansor et al. [9] studied the fatigue life behavior of the API X65 steel under cyclic loading. It was observed that the rate of crack growth was dependent on the applied load. The results showed that the effect of load ratio was less important in stable crack growth regions. Peishi Yu et al. [10] discussed the dynamic crack growth in a gas pipe of API X80 steel. The crack growth was simulated by the finite element method. The results have shown that the crack-tip-opening angle depends on the crack growth speed. Kingklang and Uthaisangsuk [11] investigated the plastic deformation and damage behavior of pipeline steel grade X65 by experimental and numerical methods.

In this research, by the experimental method, three-point bending tests were done on eight samples of gas and oil transfer pipelines made in steel API L X65 along with peripheral welding with the same geometric dimensions, same groove length, and different loading. The fracture toughness on peripheral welding was calculated based on the standard BS 7448. Also, the fracture toughness is calculated by computing simulation by using ABAQUS software v6/10 and compared to experimental results.

2   THE WELDING ZONE FRACTURE TOUGHNESS BY THE EXPERIMENTAL METHOD

To construct the example test, two the API X65 steel pipes were prepared with 48 inches diameters and standard V-shape head. The pipes were welded together in standard conditions. The view of how two pipes can be connected is shown in Fig. 1.

Fig.1
The V-shape head of the gas and oil pipe in the welding process.

The first pass (root pass) welding is done by the E6010 electrode with a 2.5 *mm* size. The root pass is the most important pass on the welding process of the pipeline because every welding penetration is done in a pass. The next welding passes were done by the E7010 electrode with a 4 *mm* size from the second one to the eighth one. After the welding process (for ensuring welding quality), the non-destructive test (such as visual test) and radiographic test were done. The exterior weld after welding and surface cleaning is shown in Fig. 2.
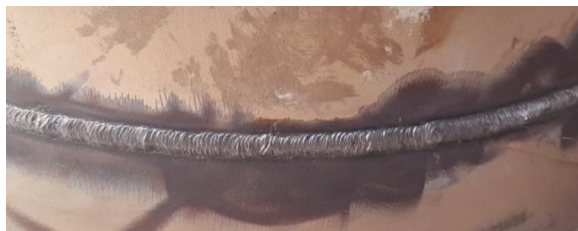
Fig.2
The Exterior weld after welding and surface cleaning.

The base metal API X65 and welding zone mechanical properties are listed in Table 1 [3]:

Table 1
API-X65 base metal and weld metal mechanical properties.

Steel	Yield strength (*MPa*)	Tensile strength (*MPa*)	Elastic modules (*GPa*)
Weld metal	530	678	212
Base metal	453	601	210

The schematic diagram of the three-point bending test specimen geometry is shown in Fig. 3, where S is the length of the sample, and B and W are the thickness and width of the sample, respectively, and a is the crack length.
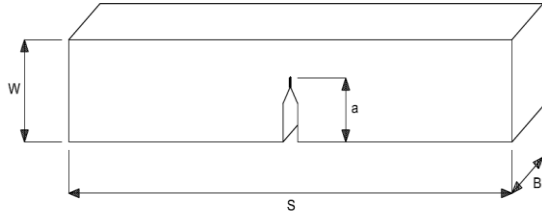

Fig.3
Schematic diagrams of the three-point bending test specimen geometry.

The samples, used for three-point bending tests, were prepared by cutting the welding zone and creating a crack on them with a wire cut machine (Fig. 4).
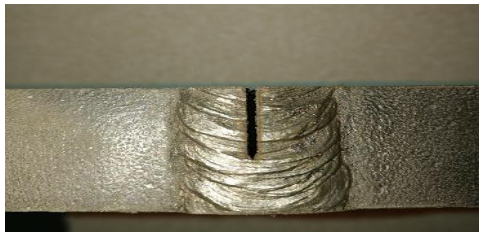
Fig.4
The slice of the welding zone with creating a crack on it.

Then, samples for a three-point bending test were prepared like Fig. 5 by geometric specifications of 120 *mm* length, 24 *mm* width, 12 *mm* thickness, and 15 *mm* primitive crack length.

Fig.5
Experimental samples before the test.

According to the BS 7448 and ASTM 7448 standards, in a three-point bending test, samples were prepared with constant dimensions, crack length, and different displacements [12]. In this research, eight samples were prepared and tested by using a Zuwick 600 *kN* testing machine (Germany). The test device during the test is shown in Fig. 6.

Fig.6
The three-point bending test device during the test.

Tests on samples were done for 1.5, 2, 2.5, 3, 3.5, 4, 4.5, and 5 *mm* displacements, and results were obtained in the form of force on the displacement chart for each sample. After a three-point bending test on samples, they must be broken on the crisp mode to determine the soft and crisp fracture border. For this purpose, samples were placed in liquid nitrogen for 15 minutes. Then, samples were fixed one by one in the clamp-on laboratory and controlled environment, and were fractured by the sudden beat hammer. Fig. 7 shows a sample that was broken after taking out from liquid nitrogen instantly.

Fig.7
A sample that was broken after taking out from liquid nitrogen.

By using an optical microscope equipped with a camera (NANBEI XTL-500), pictures were taken from each sample fracture surface. In Fig. 8, a microscopic sample image is shown for 4.5 *mm* displacement. In this image, crisp fracture surface and crack growth are obvious. Then, the amount of soft crack growth was measured from fracture surface images. The amounts of each sample crack growth are listed in Table 2.
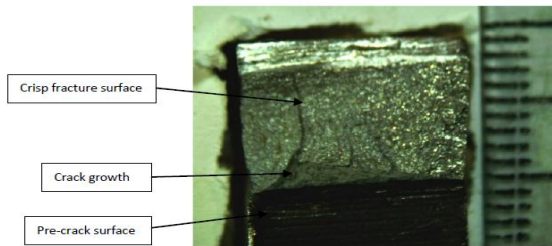

Fig.8
A microscopic sample image with 4.5 *mm* displacement.

Table 2
Amounts of each sample Crack growth.

Sample	1	2	5	4	5	6	7	8
Displacement(*mm*)	1.5	2	2.5	3	3.5	4	4.5	5
Crack growth(*mm*)	0.18	0.25	0.35	0.52	0.65	1.00	1.2	1.4

To determine the amount of *J*-integral based on standard ASTM 1820, this integral includes two parts (i.e., elastic part and plastic part). *J*-integral in a plane strain condition calculated as [12]:

$$J = J_{el} + J_p = \frac{K^2(1-v^2)}{E} + \frac{2A_{PL}}{BW} \tag{1}$$

where J_{el} and J_p are the elastic and plastic component of *J* respectively, v is Poisson's ratio, K is the mode *I* stress intensity factor, E is the elastic modulus, and A_{Pl} is the area under the force versus displacement curve as it is shown in Fig. 9.
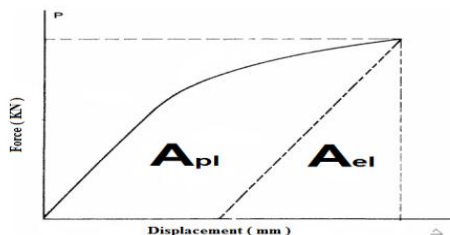

Fig.9
The area under the force versus displacement curve.

The critical stress intensity factor for this sample was computed as [13]:

$$K = \frac{P_Q S}{BW^{3/2}} f\left(\frac{a}{w}\right)$$ (2)

where P_Q is critical loading, and $f\left(\frac{a}{w}\right)$ is the shape coefficient that can be determined as [13]:

$$f\left(\frac{a}{w}\right) = \frac{3(a/W)^{1/2}\left[1.99 - (a/W)(1-a/W)(2.15 - 3.93(a/W) + 2.7(a/W)^2)\right]}{2\left[1 + 2(a/W)\right](1-a/W)^{3/2}}$$ (3)

Sample dimensions, which prepared from welding metal for the three-point bending test, are $S = 96\,mm$, $W = 24\,mm$ and $a = 15\,mm$ (Figs. 3 and 5). Thus, according to Eq. (3), the amount of shape coefficient $f(a/W)$ obtained 16.66. Samples were tested for 1.5, 2, 2.5, 3, 3.5, 4, 4.5, and 5 displacements, and force diagram, in terms of displacement, extracted for each sample. In Fig. 10, the force-displacement diagram is shown for a sample with 4.5 *mm* displacement. To determine P_Q from this diagram, a 0.95 slope line was drawn; the intersection of this line, with the force-displacement curve in the elastic zone, specifies the value of P_Q. Then *K* was calculated by Eq. (2). In addition, the determined plastic zone area and *J*-integral were calculated by Eq. (1). The results of the eight tested samples are shown in Table 3.
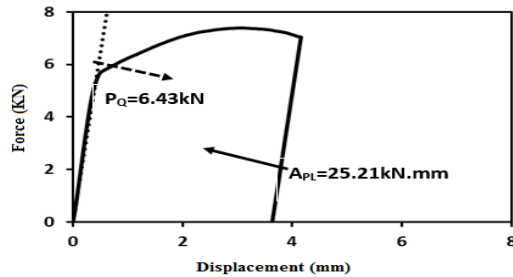

Fig.10
The force-displacement diagram for the sample with 4.5 *mm* displacement.

Table 3
The results of the eight tested samples.

Sample	Displacement (mm)	P_Q (kN)	K_I (MPa.m$^{1/2}$)	A_{pl} (kN.mm)	J_{el} (kN/m)	J_{pl} (kN/m)	J (kN/m)
1	1.5	6.58	59.1	2.88	14.99	53.33	68.32
2	2	5.87	52.6	6.64	11.87	122.95	134.82
3	2.5	5.75	51.55	10.30	11.32	190.74	202.1
4	3	6.00	53.95	13.47	12.49	249.44	261.94
5	3.5	6.74	60.40	19.10	15.65	353.15	368.8
6	4	6.33	56.75	23.45	13.81	434.26	448.10
7	4.5	6.43	57.62	25.21	14.25	466.85	481.1
8	5	6.10	54.31	28.05	12.66	519.44	532.1

After determining *J*-integral and soft crack growth for each sample, we can draw *J*-integral versus crack growth (Δa), which is shown in Fig. 11. A construction line is plotted in accordance with the equation of $J = M \sigma_Y \Delta a$, where the slope $M = 2$ or a larger *M* can be determined from the fit of the initial test data [14]. In this study, the value of *M* is assumed to be four. Then, exclusion lines were drawn parallel to the construction line intersecting the abscissa at 0.15 *mm* and 1.5 *mm*. At last, a line was drawn parallel to the construction and exclusion lines at an offset value of 0.2 *mm*. The intersection of a 0.2 *mm* offset line, with the power-law regression curve, specifies the value of J_{IC}. Accordingly, the amount of J_{IC}, which obtained in this research, is $J_{IC} = 135.5\,kJ/m^2$. After determining critical *J*-integral, the fracture toughness was calculated from Eq. (4) [13].

$$J_{IC} = \frac{(1-v^2)K_{IC}^2}{E} \qquad (4)$$

The amount of fracture toughness of welding metal was obtained as $K_{IC} = 177.5\,MPa\sqrt{m}$.
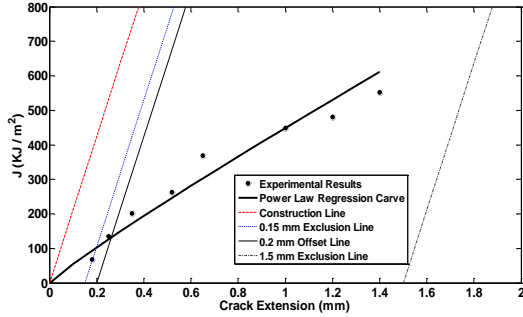

Fig.11
Material resistance curve based on *J*-integral for steel API-X65 weld metal.

3   DETERMINATION OF THE CRITICAL CRACK LENGHT

According to the obtained results, critical crack length scrutiny was calculated for base metal and peripheral welding. The critical crack length was determined as [13]:

$$a_C = \frac{1}{\pi}\left(\frac{K_{IC}}{\sigma_Y}\right)^2 \qquad (5)$$

In which a_C is the critical crack length, K_{IC} is fracture toughness, and σ_Y is yield strength. Base Metal and peripheral critical crack length comparisons are shown in Table 4.

Table 4
Base Metal and peripheral critical crack length comparisons

Material	Fracture toughness ($MPa\sqrt{m}$)	Yield strength (*MPa*)	Critical crack length (*mm*)
API-X65 Base metal	308	453	147
Welding zone metal	177	530	35

According to Table 4, the welding zone critical crack length is 76% less than the base metal. Thus, cracks up to 185 *mm* length, which is acceptable for base metal if it is created on the welding zone, are very dangerous and can be led to fracture and failure pipelines from the welding zone.

4   THE WELDING ZONE FRACTURE TOUGHNESS BY FINITE ELEMENT METHOD

Three-point bending test simulation was done by considering experimental test conditions and by ABAQUS v6/10 software. The crack tip opening displacement (CTOD) was obtained by software, and the fracture toughness was determined as [13]:

$$CTOD = \frac{(1-v^2)K_{IC}^2}{2\sigma_Y E} \qquad (6)$$

According to Fig. 12, the crack tip opening displacement (CTOD) is for cracking the sides, which defined in this form for displacement in the place of two perpendicular lines collision.
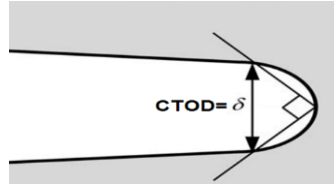
Fig.12
The CTOD definition.

In this research, the three-point bending test sample dimensionally modeled according to Fig. 13. Also, support rollers, based on the experimental test by 9 *mm* radius and hammer by 8 *mm* radius, modeled in this form of rigid.
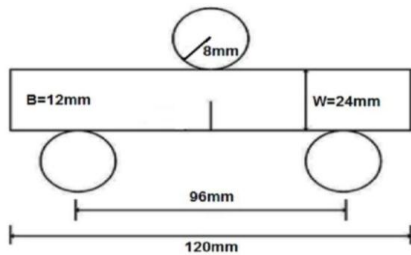

Fig.13
Sample dimensions on the three-bending test.

The material properties, such as the elastic modulus, Poisson's ratio and plastic properties were introduced to the software. Welding plastic properties were obtained based on the tensile test of the grooved specimen, which were introduced to the software by 20 pair-points. Welding plastic properties are shown in Table 5.

Table 5
Welding plastic properties that were inputted to the software.

Stress (*MPa*)	Plastic strain (*mm/mm*)
530	0
599	0.012
621	0.022
651	0.050
686	0.120
700	0.170
733	0.200
764	0.300
776	0.350
797	0.450
806	0.500
821	0.600
834	0.700
846	0.800
851	0.850
856	0.90
865	1.00

The gap between supports, based on standards, was considered 96 *mm*. (samples width quadruple). The set connection is shown in Fig. 14.
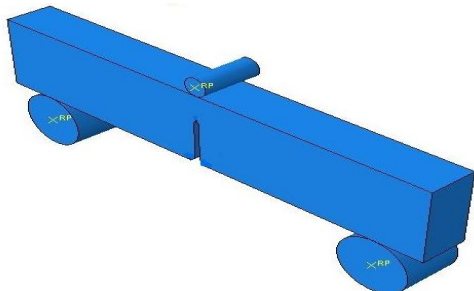
Fig.14
The set connection.

On the static pseudo, cases, such as three-point bending tests, inertia, and kinetic energies, are negligible because of low absolute magnitude speed and acceleration amounts. Therefore, in this case, simulation usually used static condition. According to the experimental test, the simulation was done as a controlled displacement by a machine with a movable jaw and low-speed (0.03 *mm/sec* speed) form. For this purpose, in the load amplitude part, a table was prepared, including two columns, the first column is time, and the second one is applied displacement and was introduced to the software. For an accurate calculation, the element around the crack was selected smaller. The networking sample dimensions on the crack growth zone were estimated at 0.2×0.2×0.2 *mm*. Because the sample was modeled three-dimensional, acting elements were chosen in rigid type and eight nodes (C3D8R). Grid models, with details around the networking crack, are shown in Fig. 15. For the sample, 25610 eight-node elements are used, and for each support 2080 elements are used. So, the number of hammer elements is 735, and the total number of set elements is 30505.
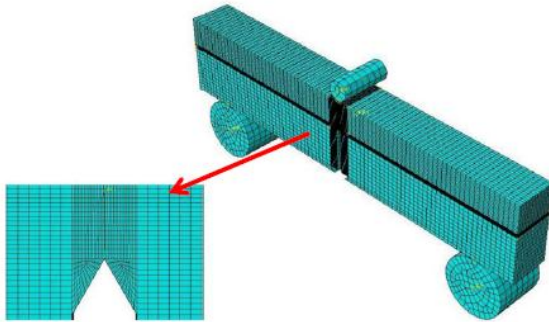

Fig.15
Grid model with details around the networking crack (C3D8R).

Fig. 16 shows that Mises tension stress, during the hammer displacement, is 5 *mm*, and the first element starts to destruction.
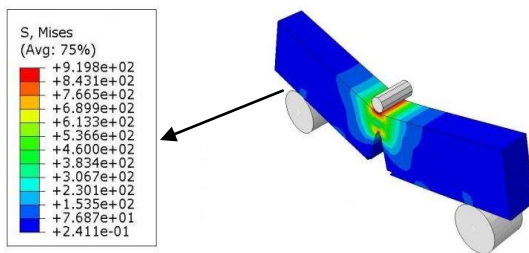

Fig.16
Mises tension contour during the first element destruction.

The amount of CTOD was achieved at 0.14 *mm*. After determining CTOD, the fracture toughness was calculated from Eq. (6). The amount of fracture toughness of welding metal was obtained as $K_{IC} = 185.9\, MPa\sqrt{m}$. Table 6 compares the results of the experimental and numerical methods. The numerical solution has a 4.7% difference from the experimental solution. Critical *J*-integral J_{IC} (*kN/m*).

Table 6
Compares the results of the experimental and numerical methods.

Method	Critical *J*-integral J_{IC} (*kN / m*)	CTOD (*mm*)	Fracture toughness ($MPa\sqrt{m}$)
Experimental methods	135.5	---	177.5
Numerical method	---	0.14	185.9
Difference between two method	---	---	4.7%

5   CONCLUSION

In this research, fracture toughness of the welding zone in gas and oil transfer pipelines (made in steel API X65) was calculated by a three-point bending test experimental method. Also, via a simulation on ABAQUS software v6/10

fracture toughness was calculated by the numerical method and compared to experimental results .The computing simulation and experimental results comparison show good matching results by the two methods. The amount of gained fracture toughness by the experimental method is $K_{IC} = 177.5 MPa\sqrt{m}$ and by the numerical method is $K_{IC} = 185.9 MPa\sqrt{m}$, which their comparison shows that the numerical solution is 4.7% different from the experimental solution .

The comparison between the amount of fracture toughness in the welding zone and base metal API X65 shows that fracture toughness of the welding zone is 43% less than the base metal. It shows that welded gas and oil pipelines have more crack growth talent compared to the base metal. Moreover, results show that the critical crack length on the peripheral welding zone is 68% less than the critical crack length on the base metal. It shows the importance of existence crack on gas and oil peripheral welding pipelines even if it has a very small size.

REFERENCES

[1]   Shin K.I., Park J.H., 2002, Simulation of stress corrosion crack growth in steam generation tubes, *Nuclear Engineering and Design* **214**: 91-101.

[2]   Kamaya M., Kitamura T.A., 2004, Simulation on growth of multiple small cracks under stress corrosion, *International Journal of Fracture* **130**(4): 787-801.

[3]   Lee J.S., Ju J.B., Jang J.I, Kim W.S., Kwon D., 2004, Weld crack assessments in API X65 pipeline failure assessment diagrams with variations in representative mechanical properties, *Materials Science and Engineering* **373**: 122-130.

[4]   Oh C.K., Kim Y.J., Beak J.H., Kim Y.P., Kim W., 2007, A phenomenological model of ductile fracture for API X65 steel, *International Journal of Mechanical Sciences* **49**: 1399-1412.

[5]   Beak J.H.,Kim Y.P., Kim C.M., Kim W.S., Seok C.S., 2010, Effect of Pre-Strain on the mechanical properties of API X65 pipe, *Material and Science A* **527**(6): 1473-1479.

[6]   Ben Amara M., Pluvinage G., Capelle J., Azari Z., 2016, Modelling crack propagation and arrest in gas pipes using CTOA criterion, *Fracture at all Scales* **2016**: 171-194.

[7]   Sirin K., Sule Y., Kaluc E., 2016, Influence of the chemical composition of weld electrode on the mechanical properties of submerged arc welded pipe, *The International Journal of Advanced Manufacturing Technology* **87**(5-8): 1941-1950.

[8]   Maksuti R., Mehmeti H., Baum H., Rama M., Çerkini N., 2017, Correlation of microstructure and toughness of the welded joint of pipeline steel X65, *Damage and Fracture Mechanics* **2017**: 315-322.

[9]   Mansor N.I.I., Abdullah S., Ariffin A.K., 2017, Discrepancies of fatigue crack growth behaviour of API X65 steel, *Journal of Mechanical Science and Technology* **31**(10): 4719-4726.

[10]   Yu P., Lu J., Zhao J., 2018, Finite element simulations of dynamic fracture of full-scale gas transmission pipelines, *Acta Mechanica Solida Sinica* **31**(3): 357-368.

[11]   Kingklang S., Uthaisangsuk V., 2018, Plastic deformation and fracture behavior of X65 pipeline steel: Experiments and modeling, *Engineering Fracture Mechanics* **191**(15): 82-101.

[12]   Standard Test Method for Measurement Fracture Toughness, 2001, E1820, ASTM.

[13]   Gdoutos E.E., 2005, *Fracture Mechanics*, Springer.

[14]   Zhu X.K., James A., 2012, Review of fracture toughness (G, K, J, CTOD, CTOA) testing and standardization, *Engineering Fracture Mechanics* **85**: 1-46.